applied sciences

MDPI

Article

Millimeter Wave Propagation Measurements and Characteristics for 5G System

Ahmed M. Al-Samman [1,*], Marwan Hadri Azmi [2], Y. A. Al-Gumaei [3,*], Tawfik Al-Hadhrami [4], Tharek Abd. Rahman [2], Yousef Fazea [5] and Abdulmajid Al-Mqdashi [6]

1 Department of Manufacturing and Civil Engineering, Norwegian University of Science and Technology, 2815 Gjøvik, Norway
2 Wireless Communication Centre, School of Electrical Engineering, Faculty of Engineering, Universiti Teknologi Malaysia, Skudai, Johor 81310, Malaysia; hadri@utm.my (M.H.A.); tharek@fke.utm.my (T.A.R.)
3 Department of Computer and Information Science, Faculty of Engineering and Environment, Northumbria University, Newcastle upon Tyne NE18ST, UK
4 School of Science and Technology, Nottingham Trent University, Nottingham NG118NF, UK; Tawfik.al-hadhrami@ntu.ac.uk
5 Internetworks Research Laboratory, School of Computing, Universiti Utara Malaysia, Sintok 06010, Kedah, Malaysia; yosiffz@uum.edu.my
6 Faculty of Computer Science and Information Systems, Thamar University, Dhamar 87246, Yemen; abdulmajid.almqdashi@gmail.com
* Correspondence: ahmed.al-saman@ntnu.no (A.M.A.-S.); Yousef.al-gumaei@northumbria.ac.uk (Y.A.A.-G.)

Received: 18 November 2019; Accepted: 19 December 2019; Published: 2 January 2020

Abstract: In future 5G systems, the millimeter wave (mmWave) band will be used to support a large capacity for current mobile broadband. Therefore, the radio access technology (RAT) should be made available for 5G devices to help in distinct situations, for example device-to-device communications (D2D) and multi-hops. This paper presents ultra-wideband channel measurements for millimeter wave bands at 19, 28, and 38 GHz. We used an ultra-wideband channel sounder (1 GHz bandwidth) in an indoor to outdoor (I2O) environment for non-line-of-sight (NLOS) scenarios. In an NLOS environment, there is no direct path (line of sight), and all of the contributed paths are received from different physical objects by refection propagation phenomena. Hence, in this work, a directional horn antenna (high gain) was used at the transmitter, while an omnidirectional antenna was used at the receiver to collect the radio signals from all directions. The path loss and temporal dispersion were examined based on the acquired measurement data—the 5G propagation characteristics. Two different path loss models were used, namely close-in (CI) free space reference distance and alpha-beta-gamma (ABG) models. The time dispersion parameters were provided based on a mean excess delay, a root mean square (RMS) delay spread, and a maximum excess delay. The path loss exponent for this NLOS specific environment was found to be low for all of the proposed frequencies, and the RMS delay spread values were less than 30 ns for all of the measured frequencies, and the average RMS delay spread values were 19.2, 19.3, and 20.3 ns for 19, 28, and 38 GHz frequencies, respectively. Moreover, the mean excess delay values were found also at 26.1, 25.8, and 27.3 ns for 19, 28, and 38 GHz frequencies, respectively. The propagation signal through the NLOS channel at 19, 28, and 38 GHz was strong with a low delay; it is concluded that these bands are reliable for 5G systems in short-range applications.

Keywords: 5G; 19 GHz; 28 GHz; 38 GHz; NLOS; path loss; RMS delay spread

1. Introduction

The spectrum with a range of 1–100 mm (3–300 GHz band) wavelengths can be classified as millimetre-Wave (mm-Wave) bands [1,2]. There is an excellent interest in short range communications using mm Waves (mmWave) [3–6]. Because of their mainly unaccredited or light-licensed bandwidth, these bands are now promising applicants for next-generation wireless communication, such as device-to-device (D2D) communications [7]. Millimeter wave spectrum bands for 5G were also identified by the World Radio Conference (WRC) 2015 [8], and are expected to be finalized by WRC 2019.

Many researchers have studied the characteristics of the wideband channel in different frequency bands in order to meet high data-rate demands. For a wideband channel at a low frequency band, in the early 2000s, Durgin et al. [9] studied angle delaying and dispersion characteristics in the case of an indoor peer-to-peer (P2P) channel centered at 1920 MHz. In the work, the omnidirectional and directional antennas for measuring the angles of arrival and delay propagation statistics have been used. The typical results for the root mean square (RMS) delay spreads were 17–219 ns for the outdoor cross-campus measurements, and three indoor-to-indoor locations exhibited 27–34 ns RMS delay spreads and normalized angular spreads of multipath power between 0.73 and 0.90 [9]. Recent measurement campaigns were conducted to obtain propagation measurements and channel modeling at 28, 38, 60, and 73 GHz in an urban microcell, urban macrocell, rural area, indoor hotspot, and vehicle scenarios, respectively [10–13]. In the literature [14], the measurements were carried out in rural and urban locations at frequency bands of 50 MHz–6 GHz. Alvarez et al. [15] used an indoor radio channel over a range of 1–9 GHz, using omnidirectional antennas and four environments (line-of-sight (LOS), soft non-LOS (NLOS), hard NLOS, and a corridor). The path loss exponents (PLEs) with verity reference distances were high in the hard-NLOS scenario compared with the others [13,15,16]. Additionally, Shu Sun et al. studied indoor propagation measurements at 2–73 GHz in LOS and NLOS for offices and shopping malls, and the measured path loss as a function of distances [13]. They have carried through measured information and ray tracking of 28 to 73.5 GHz in the mmWave frequency bands, comparing trajectory models. Their work revealed that the studied path-loss models were very comparable in their prediction accuracy, given large datasets, even though some of these models required more model parameters and lacked a physical basis for their floating intercept value. Indoor channel propagation studies are reported in [17–19], while outdoor channel propagation studies are reported in [20–22], as listed in Table 1. Wang et al. [16] carried out 26 GHz open office LOS measurements of the wideband channel. In the literature [18], the first sounding channel and the original outcomes are provided for synthesized omnidirectional findings of the 28 GHz band. In the literature [19], in a line-of-sight (LOS) situation, mmWave propagation features were studied in 6.5, 10.5, 15, 19, 28, and 38 GHz bands in the indoor corridor setting. For outdoor cellular propagation, the world's first empirical measurements were conducted at 28, 38, and 73 GHz in New York [20–22].

Table 1. Overview of some outdoor and indoor studies at millimeter wave bands.

Source	Environment	Frequency (GHz)	Bandwidth (MHz)	Distance (m)	Parameters of Study
Wang et al. [17]	Indoor	26	1000	2–67	Path loss, delay, and angular spreads
Hur et al. [18]	Indoor	28	250	–	Power delay profile
Al-samman et al. [19]	Indoor	6.5–38 GHz	1000	1–40	Path loss and delay spread
Azar et al. [20]	Outdoor	28	400	30–500	Path loss and power delay profile
MacCartney et al. [21]	Outdoor	28 and 38	400	50–200	Path loss
Sun et al. [22]	Outdoor	28 and 73	400	27–190	Path loss

While propagation studies for the coexistence of 5G in the mmWave bands have been aggressively performed for some time, the characterization of the 5G channel model still requires further investigation. This is because most of the measurement campaigns are conducted using different settings, including measurement environments; morphologies; equipment like channel sounder, antennas, and clock synchronization; and even the post-processing method, which may influence the propagation characteristics. As a result, more mmWave channel measurements and characterizations are still needed in order to fully characterize and later develop a unified channel model framework for large mmWave bands. To fill the aforementioned gaps, we carried out an extensive mmWave channel measurement campaign on a particular NLOS indoor-to-outdoor (I2O) scenario, covering frequencies of 19, 28, and 38 GHz. The contributions of this paper are threefold. First, this work compares the propagation characteristics of different mmWave frequency bands, where the 19, 28, and 38 GHz channel measurements are carried out with the same configuration. In addition, the measurement campaign is conducted using a 1000 mega chips-per-second (Mcps) high-band correlation channel with a greater chip-rate than the measurement conducted in the literature [2,16,23,24]. The second contribution of the paper is the study of path loss for a single frequency based on the close-in (CI) space-lost reference path model, while the path loss for the multi-frequency is based on CI and alpha–beta–gamma (ABG) models. Finally, the third contribution constitutes of the computation of the root mean square (RMS), the average excess (MN-EX), and the maximum excess delays (MAX-EX), to characterize the time dispersion parameters for all of the measured frequencies.

The rest of this article is structured accordingly. The measurement method and environment are described in Sections 2 and 3, respectively. The post processing of the data is explained in Section 4. Sections 5 and 6 discuss and analyze the path-loss patterns and time dispersion parameters, and provides the outcomes and discussions, respectively. In Section 7, this work is compared with the state of art. The conclusion of the paper is drawn in Section 8.

2. Measurement Technique

This section describes the configuration of the equipment of the 5G channel sounder that was used for our experiment. The time domain measurements were conducted in an I2O NLOS environment at 19, 28, and 38 GHz frequencies. The block diagram of the measurement equipment is shown in the Figure 1. An arbitrary waveform generator (AWG) was applied to a transmitter (Tx). The receptor (Rx) was equipped with a 12-bit (1 GHz bandwidth) high-speed digitizer (Rx) for the acquisition of a sound signal. At the transmitter, the AWG transformed a radio frequency (RF; up to 44 GHz) carrier with broad modulation bandwidth from the produced differential basis band in-phase quadrature (IQ), using an E8267D PSG up converter. The down-converter M9362AD01 PXIe was used to convert the RF frequencies (up to 40 GHz) to the intermediate frequency, the IF signal was amplified by an M9352A hybrid amplifier/attenuator (500 MHz), and the IF signal was lastly acquired using the interlocking mode with the M9703A 12-bit 1 GHz bandwidth high-speed numbers. The local down converter oscillator (LO) was used with an N5173B EXG. Two rubidium clock devices (one for Tx and one for Rx) were used to synchronize the transmitter with the receiver, providing a high generation l0 MHz referring signal for all of the devices with $\leq 10^{-11}$ accuracy and $\leq 3 \times 10^{-11}$ stability. The function generation system (Trigger box) was used to derive the trigger signals. Additional details of the measurement hardware can be found in the literature [25]. A 12-bit high speed digitizer M9703A was used for the sounding signal acquisition, which can provide one channel 1.6 G Sa/s (625 MHz bandwidth), or four channels 3.2 G Sa/s interleaving acquisition (1 GHz bandwidth) [26].

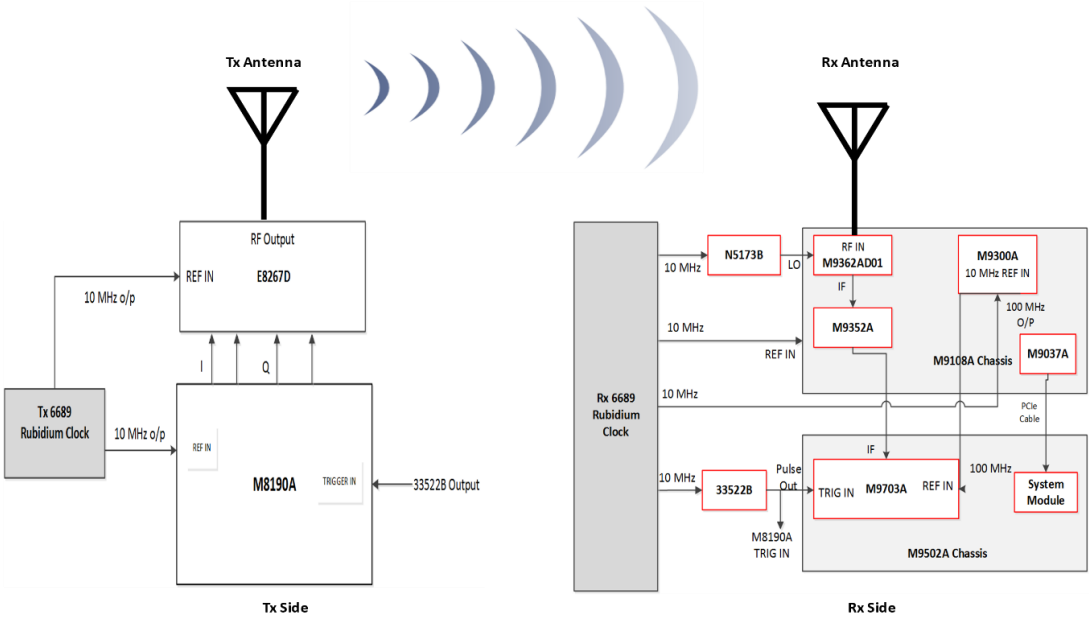

Figure 1. Block diagram of transmitter (Tx) and receptor (Rx) components for a 5G channel sounder.

The AWG yielded a 1-ns multipath resolution from a 1000 Mcps with sample rate of 7.2 GHz. We used a signal generator (up-converter) to generate the center frequencies at 19, 28, and 38 GHz with a transmitted power of 0 dBm. The signal was transmitted through a 11.6 dBi gain (39.9°/49.9° azimuth/elevation half-power beamwidth (HPBW)), a 11.6 dBi gain (39.7°/49.7° azimuth/elevation HPBW), and a 15.2 dBi gain (29.6°/29.7° azimuth/elevation HPBW) ETS-Lindgren horn antenna for the 19, 28, and 38 GHz frequencies, respectively. At the receiver, an omnidirectional antenna (3 dBi gain) with a relatively high gain power amplifier of 37 dB was used to collect the received signal.

3. Testbed of Experiment

The measurements were carried out at the Universiti Teknologi Malaysia, Kuala Lumpur (UTM-KL) campus, in an indoor to outdoor setting at the Menara Tun Razak Building. The specific I2O environment consisted of corridors surrounded by open and closed offices, conference rooms, and meeting rooms. The floor plan and pictures of the measurement environment are shown in Figure 2a,c. The study environment contained corridors that had two open ends (to the north and the south), as shown in Figure 2a. Figure 2b shows corridor A, where the the Tx antenna was placed, which was open from the north side, and curved to corridor B from the other side. Corridor B, where the Rx was placed, extended from corridor A, and was open from the south side, as shown by Figure 2c. Each of the corridor's walls were made up of a multitude of materials, including concrete, colored glass, and wood. The floor was coated with glazed ceramic tiles, and ribbed metal was formed on the ceilings of the hallways. The Tx antenna (1.7 m in height) was located in corridor A beside a concrete pillar. The direction of the Tx horn antenna is indicated in Figure 2b (toward corridor A, in the direction of the stairs and concrete pillar beside it). The Rx antenna (1.5 m in height) was an omnidirectional antenna located in corridor B at the back of the Tx antenna, as shown in Figure 2c, which rendered the environment completely NLOS. The first location of the Rx antenna was 3.7 m away from the Tx horn antenna. The Rx was then moved by 1 m to the end of corridor B; the Tx–Rx separation distance was then 13.5 m. The measurement configuration is shown in Figure 2a (left side).

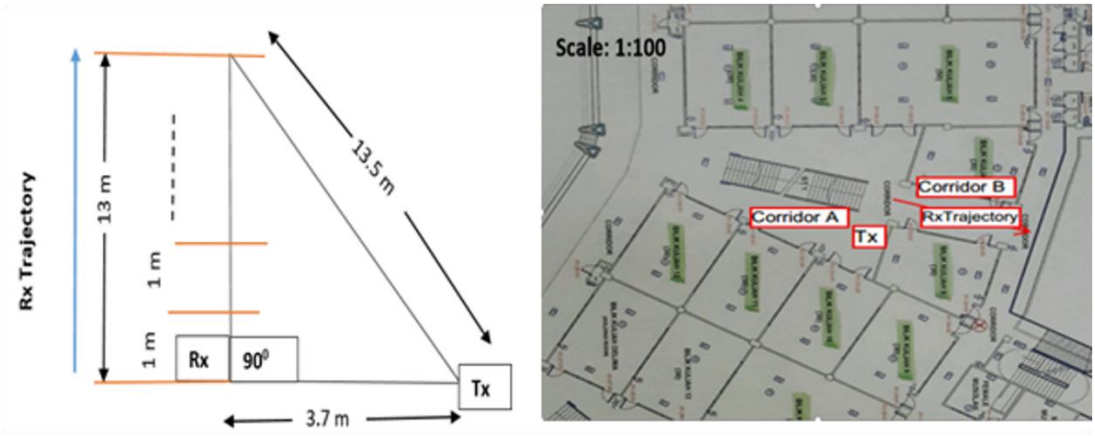

(**a**): Floor Plan

(**b**): Corridor A

(**c**): Corridor B

Figure 2. Measurement environment. (**a**) floor plan, (**b**) Tx location in Corridor A, and (**c**) Rx location in Corridor B.

4. Post Processing

This section explains the post processing of the raw data that were collected from the ultra-wideband channel sounder measurement. It includes the extraction of the channel impulse responses from the received waveforms. The data were subjected to post processing using SystemVue software [27] and MATLAB Toolbox. The channel impulse response (CIR) was extracted by cross correlation between the received waveform and the transmitted arbitrary waveform signal. the space-alternating generalized expectation-maximization (SAGE) algorithm [28,29] was used to extract the parameters of the MPCs, including the path delay and path gain. It allowed an iterative determination of the maximum-likelihood estimation. The SAGE algorithm resolved the MPCs by an interference-cancellation, where the MPCs that were already estimated were subtracted from the considered signal.

5. Path-Loss Models and Analysis

We investigated different path-loss models for single and multiple frequencies. For a single frequency, we used the CI free space reference range model [16], as follows:

$$P_L^{CI}(f,d)[dB] = P_L(f,d_0) + 10n\ \log_{10}\left(\frac{d}{d_0}\right) + W_\sigma, \quad (1)$$

where $P_L(f,d)$ is the path loss at operating frequencies, with multiple separation ranges; n is the path-loss exponent (PLE); $P_L(f,d_0)$ is the path loss in dB at a close-in (CI) range, d_0, of 1 m; and W_σ is a zero-mean Gaussian-distributed random variable with standard deviation σ dB (shadowing impact).

The other model, with three parameters, is known as the ABG model. It includes a frequency-dependent term, γ; a distance-dependent term, α; and an optimization factor, β, to describe the path loss at various frequencies [13,21,30]. The ABG model equation is given by the following [13]:

$$PL^{ABG}(f,d)[dB] = 10\alpha \log_{10}\left(\frac{d}{d_0}\right) + \beta + 10\gamma \log_{10}\left(\frac{f}{f_{ref}}\right) + W_{\sigma}^{ABG} \quad (2)$$

The minimum mean square error (MMSE) is the strategy by all of the parameters for the CI and ABG path-loss models [16].

The CI and ABG path-loss models for all of the measured frequencies are shown in Figure 3a–c.

Figure 3a shows the variation in path loss and the Tx–Rx separation distance (scatter plot and best-fit CI model at 19 GHz in NLOS environments). The path loss varies as a function of distance, based on the number of multipath components (MPCs) with their gain. The constructive and destructive nature of MPCs induces changes in the path loss. Based on the PLEs for CI and ABG (n = 0.4 and α = 0.2) at 19 GHz, the environment represents a waveguide in which many reflected paths are added constructively. Moreover, the reflected paths have a higher power because of reflections from the surrounding environment, which derive from the concrete stairs, walls, and ribbed metal ceiling; the Tx horn antenna is directed toward the stairs. Figure 3a shows that the CI and ABG models totally matched at 19 GHz for the last locations (above a 7 m Tx–Rx separation distance).

The path loss variation as a function of the Tx–Rx separation distance at 28 GHz is shown in Figure 3b. It can be noted that the fluctuations in path loss as a function of distance are the same as those shown in Figure 3a for 19 GHz. However, the path-loss measurement values increase as the frequency increases. The value of PLEs for CI and ABG models (n = 0.8 and α = 0.2) are also low, which indicates that the total power of the received signal is strong and decays minimally with distance (waveguide effects due to the physical structure of the environment). At 28 GHz, there is divergence between both CI and ABG models; however, the divergence becomes low above a 7 m separation distance, as shown in Figure 3b.

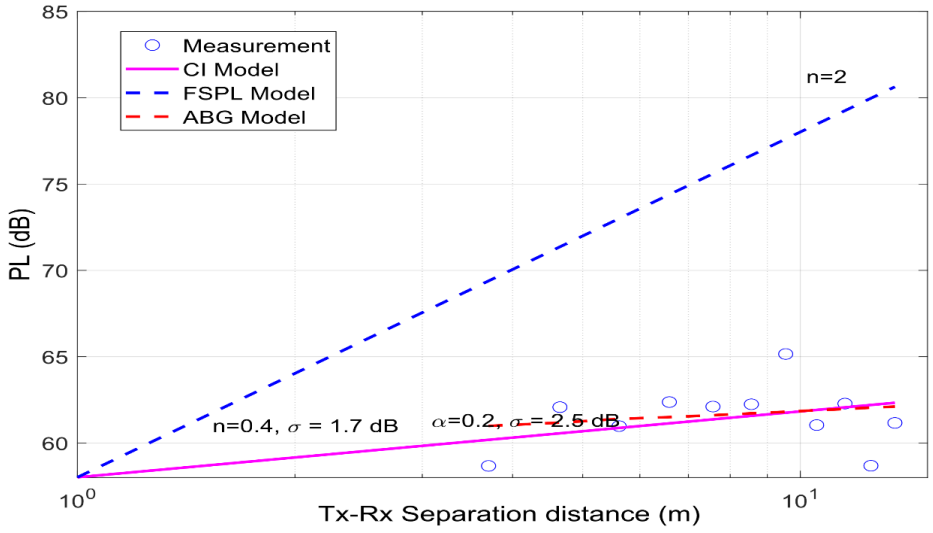

(**a**): Close-in (CI) model at 19 GHz.

Figure 3. *Cont.*

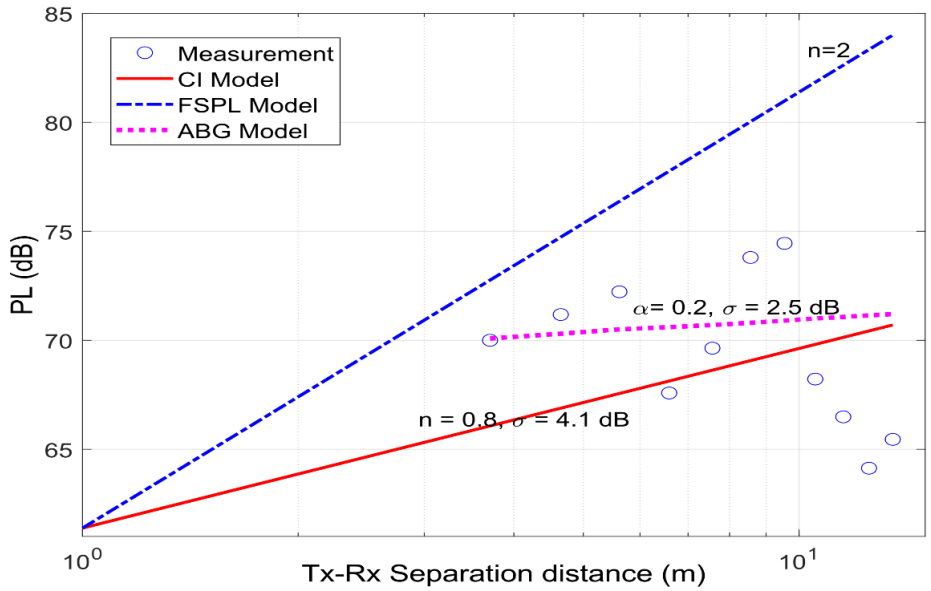

(**b**): CI model at 28 GHz.

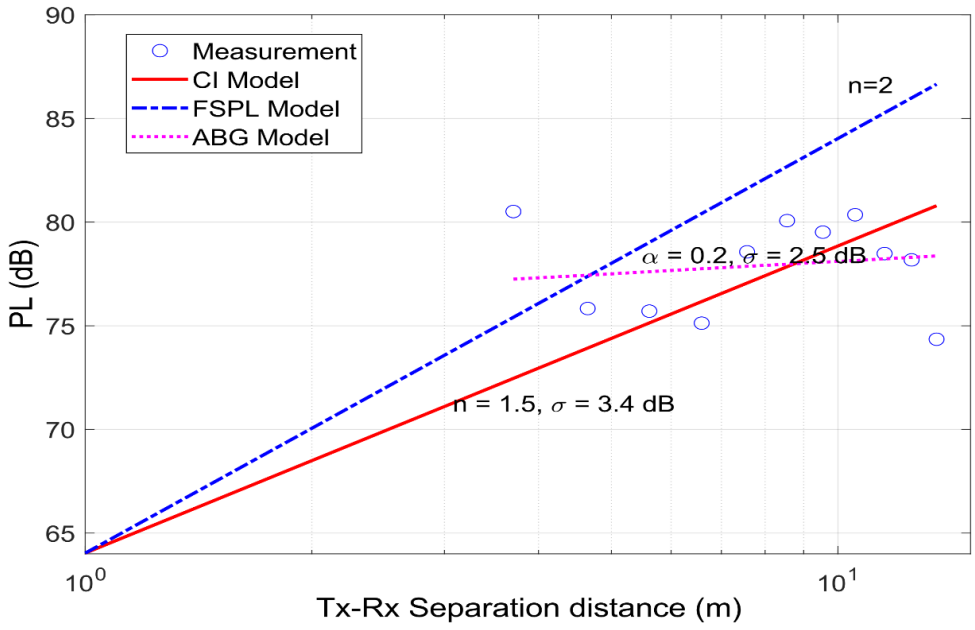

(**c**): CI model at 38 GHz.

Figure 3. Path loss versus Tx–Rx separation distance using horn-omnidirectional antennas for the soft non-line-of-sight (NLOS) environment.

Figure 3c illustrates the path loss variations as a function of the separation distance at 38 GHz. This figure shows that the path-loss measurement values at 38 GHz exceed those at 19 and 28 GHz, due to the higher frequency. The PLE for the CI model is higher compared with the PLE for the CI models at 19 and 28 GHz. However, it is still low compared with the theoretical free-space PLE (FSPL = 2), due to the constructive phenomena of MPCs and the waveguide effects induced by the concrete walls, stairs, ribbed metal ceiling, and iron railing of the corridor, which surround the Rx and Tx antennas.

According to above test, it is shown that measured data for a 38 GHz band at an I2O environment are comparable to the CI and ABG models.

Here, the ABG model has a high deviation from the CI model at all locations of measurement. This implies that the ABG model is not recommended for a 38 GHz band at an I2O environment. Hence, when we lumped different frequencies from different bands (such as from 10, 20, and 30 GHz), it is recommended to use a CI model as well for the multi-frequency scheme.

Table 2 lists the parameter values for the CI and ABG path-loss models that are used to investigate the multiple frequencies for the 5G channel propagation in this work. The CI path loss model of Equation (1) can be used for multi-frequency schemes by putting all of the measurement data for all of the measured frequencies as one data set to find an overall PLE based on all of the potential frequencies measured. The PLE for the CI model in multi-frequencies is 0.9, which is calculated based on the CI model in Equation (1) by using the MMSE approach under multiple regressions with three independent parameters—frequency, distance, and path loss.

Table 2. Multilateral path loss models 19, 28, and 38 GHz; CI; and alpha–beta–gamma (ABG) model parameters.

Model	**PLE**		**σ**	
CI	**0.9**		**5.2 dB**	
	α	β	γ	σ
ABG	0.2	5.8	5.4	2.5 dB

It can be concluded that the high-frequency propagation channels in this specific I2O environment experience constructive interference from the ground, wall, and ceiling reflections. Furthermore, one should note the radical change in the path-loss values for all of the frequencies at the last two Rx locations, due to reflections from the iron railing of the corridor. The PLE at the proposed frequencies increases with frequency. The PLE at 28 GHz is double that at 19 GHz, and the PLE at 38 GHz is about twice that at 28 GHz. This finding indicates that the PLE is frequency-dependent in this specific I2O environment. The standard deviations of the CI path-loss model are 1.7, 4.2, and 3.4 dB, for 19, 28, and 38 GHz, respectively. The standard deviation of the CI model is low at 19 GHz, which indicates that the CI model has the best agreement with the measurement data. The standard deviation values at 28 and 38 GHz are more due to the rapid fluctuation of the received signal in some constructive measurement points. The rapid changes in the measured received signals are observed at 28 GHz, as shown in Figure 3b.

Based on the path-loss models' parameters, as listed in Figure 3 and Table 2, we can conclude that the wireless signal can pass through the NLOS environment with a low signal power drop, using the huge available bandwidth in high frequencies of 19, 28, and 38 GHz.

6. Time Dispersion Parameters and Analysis

We have been investigating the time characteristics of a 5G scheme by using the RMS delay diffusion, the mean delay (MN-EX), and the maximum delay excess (MAX-EX). The MAX-EX delay is the delay where the farthest MPCs can be obtained with the gain power above the threshold value (20 dB less than the maximum power of the MPCs). The time dispersion parameters provide delay information for the channel, which is very useful for designing a robust 5G system. It is possible to calculate the RMS delay spread by the square root of the second moment of the power delay spectrum, as follows [31]:

$$\tau_{rms} = \sqrt{E(\tau^2) - (E(\tau))^2}, \tag{3}$$

where

$$E(\tau^2) = \frac{\sum_j p(\tau_j) \cdot (\tau_j)^2}{\sum_j p(\tau_j)}, \tag{4}$$

and the MN-Ex is given as follows:

$$E(\tau) = \frac{\sum_j p\left(\tau_j\right) \cdot \tau_j}{\sum_j p\left(\tau_j\right)}, \tag{5}$$

where $p\left(\tau_j\right)$ is the power of the multipath with delay τ_j.

To investigate the temporal dispersion, the received power at all of the receiver locations is depicted in Figure 4a–c, with excess delay. The Rx is indexed from 1 to 11, as shown in Figure 4a–c. For all of the measurement points at all of the investigated frequencies, most of the received power arrived at an excess delay of less than 30 ns, and between 50 to 60 ns. It can be shown that the high received power can be collected at the large excess delay for all of the measured frequencies. As an example, the Rx 6–Rx 11 have a high received power at an excess delay between 55 ns and 60 ns at 19 and 28 GHz, as shown in Figure 4a,b, and almost all of the Rx 1–Rx 11 received a high power at 38 GHz, as shown in Figure 4c. The maximum excess delay values (the delay of the received signal with power more than the noise floor of −120 dBm) are less than 93, 85, and 76 ns at 19, 28, and 38 GHz, respectively. It is worth noting that there is no linear correlation between the Rx distance, excess delay, and received power. This means that the composition of the setting plays a crucial role in 5G wireless channel at mm-wave bands. In other words, the reflection and scattering phenomena can be exploited at mm-wave frequencies to get a strong power from the farthest multipath components.

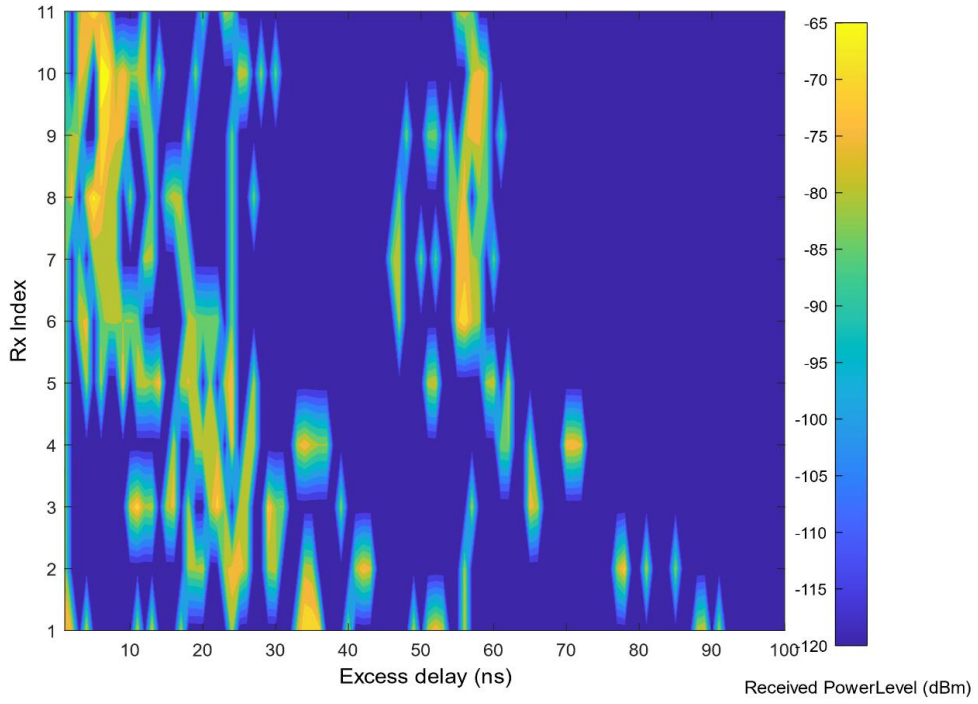

(**a**): Received power at 19 GHz.

Figure 4. *Cont.*

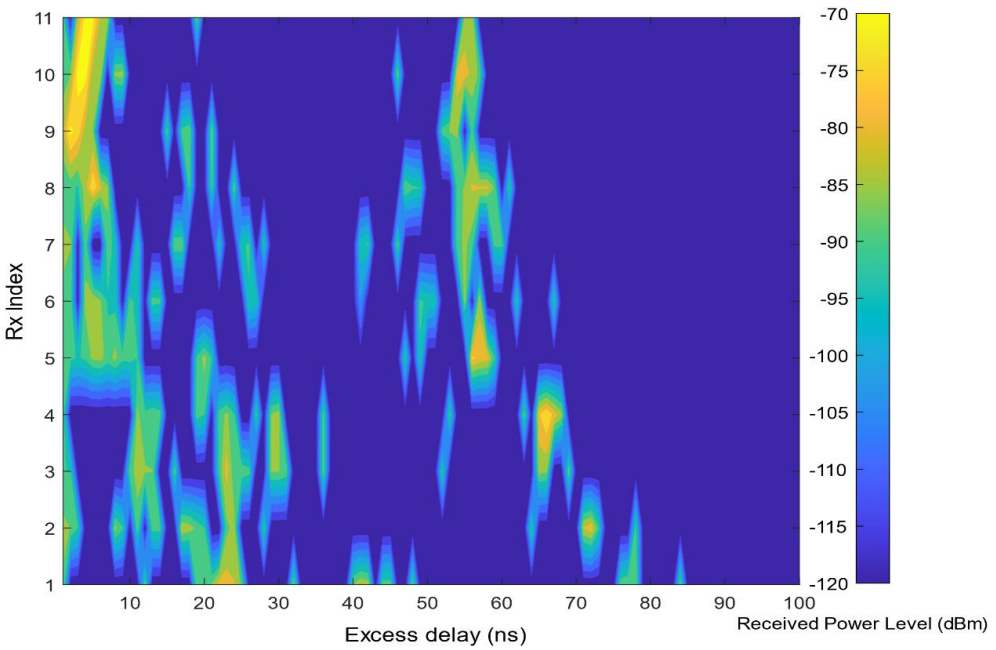

(**b**): Received power at 28 GHz

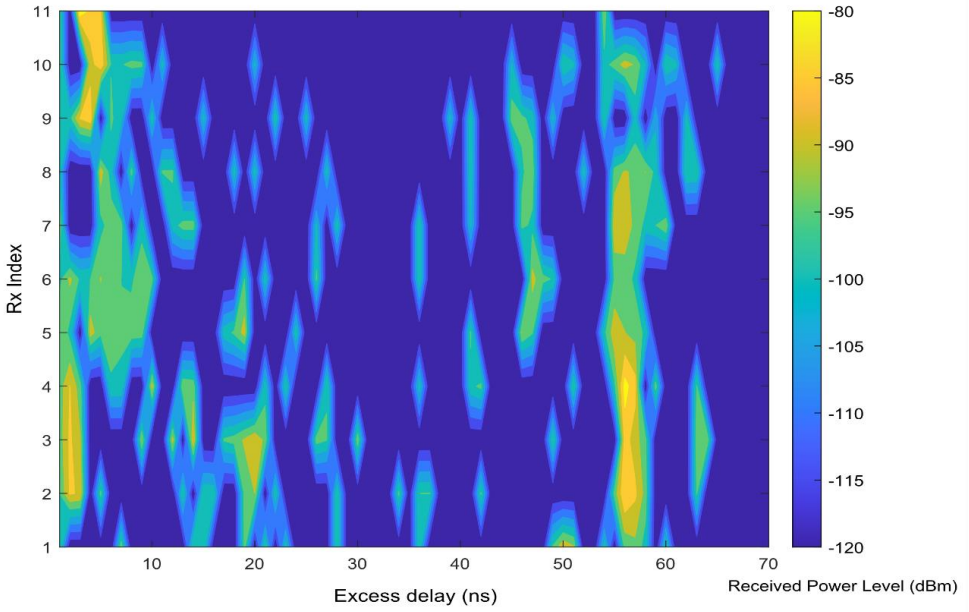

(**c**): Received power at 38 GHz.

Figure 4. Received power level versus excess delay at all of the receiver sites.

From the received power, excess delay, and using Equations (3) and (4), the temporal dispersion can be investigated based on the RMS delay spread. Figure 5 shows the RMS delay spread variation as a function of the Tx–Rx separation distance at 19, 28, and 38 GHz. Figure 5a–c shows that the RMS delay spread variation with a Tx–Rx separation distance is not linear. Moreover, the correlation between these parameters is weak, if it exists at all. The RMS delay spread at the farthest location (Tx–Rx separation distance = 13.5 m) has the lowest value at all of the frequencies (Figure 5a–c). This result implies that the farthest MPCs have less power than the threshold value (20 dB less than the maximum

power of the MPCs). Table 3 lists the values of the maximum excess delay, the mean values of RMS delay spread and mean excess delay, and the MN-EX/RMS delay spread for all of the frequencies. The MAX-EX delay varies between 64 and 90 ns; the lowest value is associated with the highest frequency. This finding indicates that, at high frequencies within the same threshold, the paths after the MAX-EX delay are ignored, because the power of these components is less than or identical to that of the noise floor. The RMS delay spread values for all of the frequencies vary between 9.2 and 29.2 ns, with mean values of 19.2, 19.3, and 20.3 ns at 19, 28, and 38 GHz, respectively. The MN-EX/RMS delay spread in this environment was more than 1, and all of the frequencies have the same value of 1.3. Based on these findings and the results in Figure 4a–c, it can be concluded that many of the strong paths arrived after the midpoint of the power delay profile and the early excess at less than 30 ns.

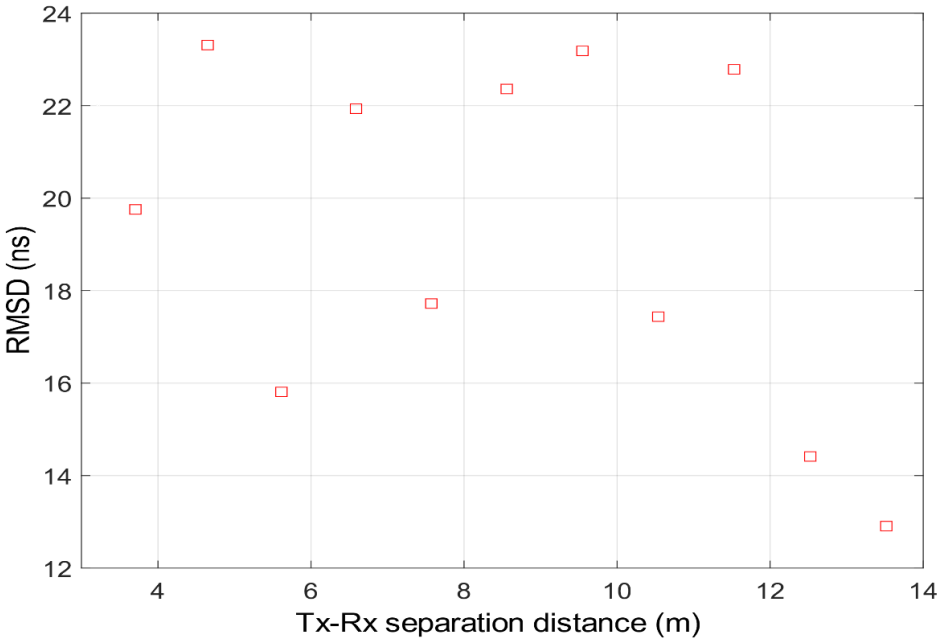

(**a**): Root mean square DS (RMSDS) at 19 GHz

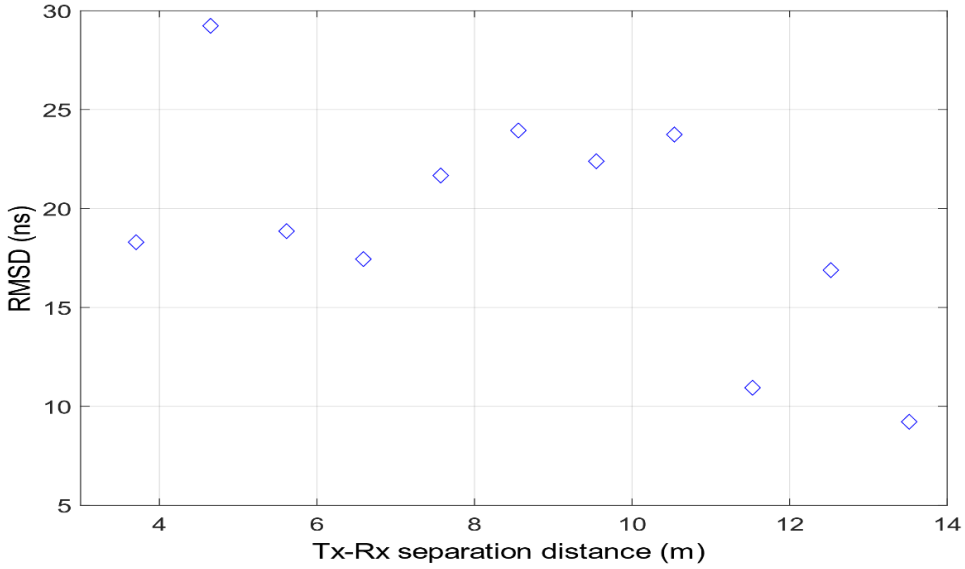

(**b**): RMSDS at 28 GHz

Figure 5. *Cont.*

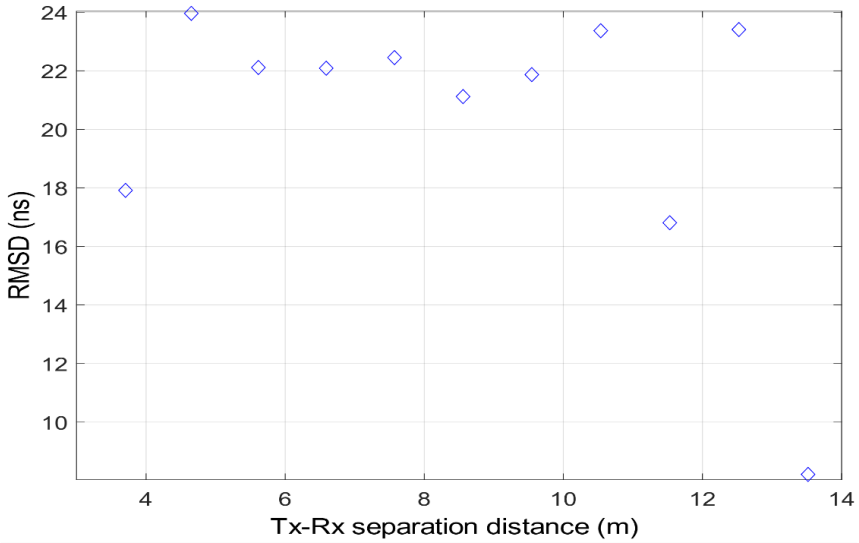

(**c**): RMSDS at 38 GHz

Figure 5. RMS delay spread (RMSDS) in the NLOS environment as a function of Tx–Rx separation.

Table 3. Maximum excess delay; mean, minimum (min), and maximum (max) RMS delay spread; MN-EX delay; and mean/delay spread (MN/RMS) for the measured frequencies.

Frequency [GHz]	MAX-EX [ns]	Mean of MN-EX [ns] (min, max)	Mean of RMS Delay Spread [ns] (min, max)	MNEX/RMS
19	90	26.1 (8.1, 42.7)	19.2 (13.0, 23.3)	1.3
28	83	25.8 (4.2, 57.0)	19.3 (9.2, 29.2)	1.3
38	64	27.4(3.7, 27.4)	20.3 (8.2, 23.4)	1.3

For the RMS delay spread results and spreading factor, it can be concluded that the time dispersion parameters are more symmetrical in the earliest MPCS compared with the latest MPCs.

Figure 6a–c illustrates the effect of path loss on the RMS delay spread at 19, 28, and 38 GHz. From these figures, it can be observed that the linear relationship between the RMS delay spread and path loss is very low. Figure 6a shows that at 19 GHz, the highest path loss is 65.2 dB at an RMS delay spread of 23.2 ns. The lowest RMS delay spread is 12.9 ns at a path loss of 61.2 ns. The lower path loss is 58.7 dB at an RMS delay spread of 14.4 ns. Figure 6b shows that at 28 GHz, the lowest RMS delay spread is 9.2 ns at a path loss of 65.5 dB. The heighest path loss is 74.5 dB at an RMS delay spread of 22.4 ns. The maximum RMS delay spread is 29.2 ns at a path loss of 71.2 dB. Figure 6c shows that the maximum RMS delay spread is 24 ns at a path loss of 75.8 ns. The maximum path loss is 80.5 dB at an RMS delay spread of 17.9 ns. The minimum RMS delay spread is 8.2 ns at a path loss of 74.4 dB. It is worth noting that in some locations, more power is acquired with a low RMS delay spread, which is very useful for 5G communication systems regarding the high information rate, to avoid intersymbol interference (ISI).

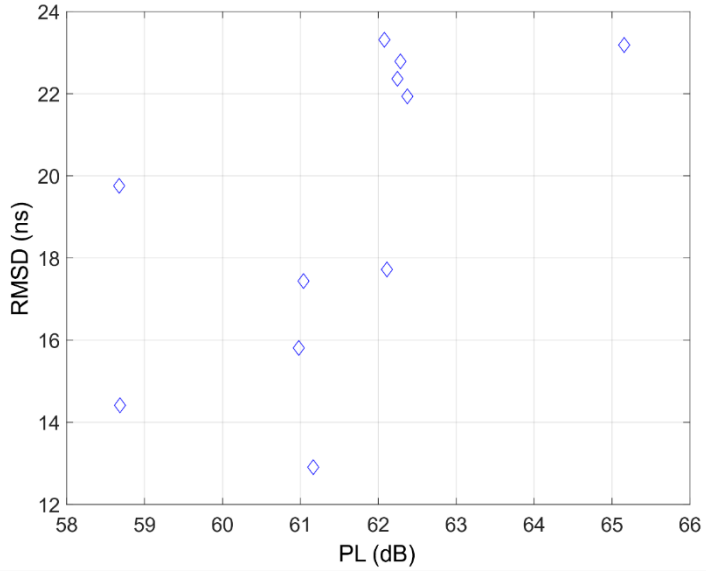

(**a**): RMSD variation with path loss at 19 GHz.

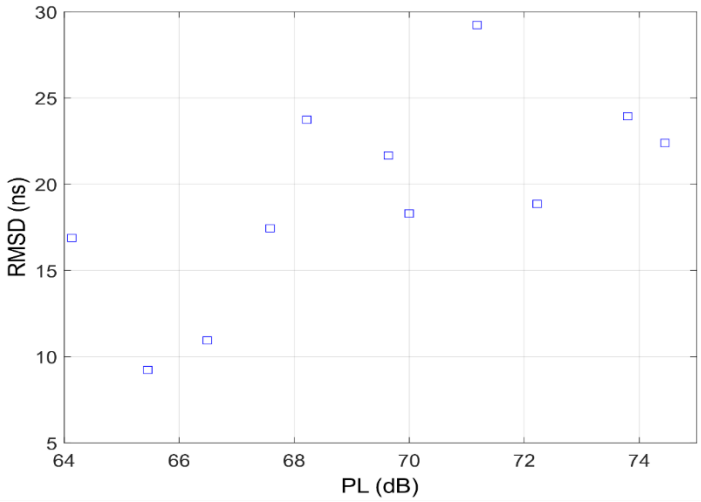

(**b**): RMSDS variation with path loss at 28 GHz.

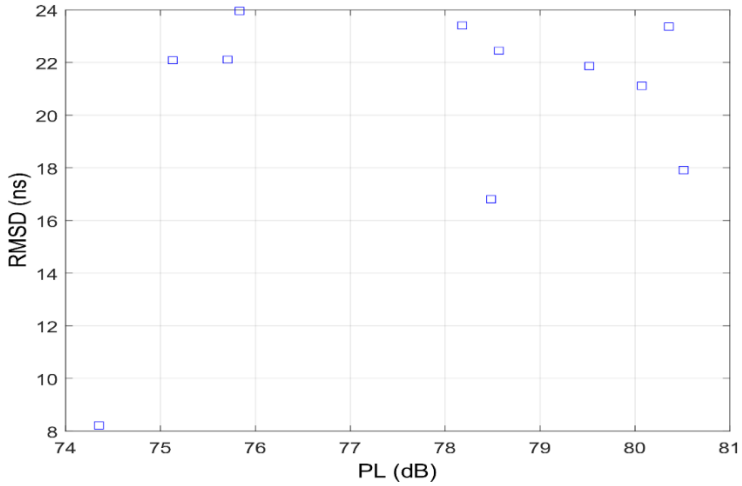

(**c**): RMSDS variation with path loss at 38 GHz.

Figure 6. The spread of RMS delay as a function of path loss.

7. Comparison with Some Studies

In this section, the path loss model extracted parameters and RMS delay spread are compared with some previous studies of 5G propagation channel models for different environments and scenarios. Because of the inherent differences in the modeling methodology—for example, the threshold employed in the algorithms of post processing and the measurements range—these parameters may not be directly comparable. However, the effect of the environments on the channel characteristics can be observed from the similarities and contrasts in different propagation models. The path loss exponent, standard deviation, RMS delay spread, and some auxiliary parameters in this work are compared with some literature in Table 4. In Table 4, the values of the propagation parameters are reported within range (lower–upper), implying that the propagation studies of the listed works provide different LOS and NLOS scenarios (single frequency, multi-frequencies, vertical and horizontal and combined antenna polarizations, environment partitioning, and directional and omnidirectional model). The lower range of PLEs (n) is identical for all of the studies. In this study, the lower range of PLE is 0.4 in the outdoor environment (LOS scenario) at a 19 GHz frequency, indicating that the MPCs added up constructively from both side walls along the outdoor office (a waveguiding effect), and the antenna has a wide-beam at this frequency, which can collect more paths. The upper range of the PLE is 1.5 at 38 GHz for the NLOS scenario in the outdoor environment. In the literature [32], the largest upper PLE (n = 4.6) is reported at 38 GHz for an NLOS outdoor environment. In the literature [27], the PLE (n = 1.89) is reported at 28 GHz for a LOS outdoor environment. In the literature [15], the largest upper PLE (n = 4) is reported at 73 GHz for vertical-horizontal polarization in an open plan (large hall) indoor environment. However, in this work, the upper PLE (n = 1.5) is investigated at 38 GHz for an I2O environment. This value indicates that the PLEs for all of the frequencies are lower than the FSPL exponent of 2, because of constructive interference and the wave guiding effects of the radio wave propagation along the studied environment. Note that the reported values of the ABG model parameter results are in consonance with the reported values in the literature [15]. Similarly, the RMS delay spread values are also in consonance with the mean values of the RMS reported results in the literature [33].

Table 4. Comparison of propagation studies for path loss models and RMS delay spread for 5G channels at mmWave bands.

Source	Frequency Range (GHz)	Distance (m)	PLE (n)	α	β	γ	σ_{CI}, σ_{ABG} (dB)	τ_{rms} (ns)
Deng et al. [33]	28, 73	4.1 21.3	1.1–3.5	–	–	–	1.7–9	4.1–21.2
MacCartny et al. [15]	28, 73	4.1 21.3	1.1–3.5	0.9 1.1	17.7–47.1	2.5–3.5	1.8–8.6, 1.8–14.2	0.5–143.8
Rappaport et al. [32]	38, 60	19–265	1.9–4.6	–	–	–	–	<122
Rajagopal et al. [27]	28, 40	≤100	1.89	–	–	–	–	
Ours	19, 28, 38	<15	0.4–1.5	0.2	5.8	5.4	1.7–4.1, 2.5	8.2–29.2

8. Conclusions

We have described the large-scale path loss in a 5G network for a wideband channel, in a specific indoor to outdoor environment measurement campaign conducted at the UTM-KL campus. We investigated path loss based on the CI and ABG path-loss models for single and multiple frequencies. For all of the measured frequencies, we provided an RMS delay spread, mean excess delay, and maximum excess delay. We recovered a good value for the PLE for all of the frequencies, using the CI path-loss model. The smaller value of the distance-dependent factor indicates that the drop in the received power is low for the measured distance in this particular NLOS-I2O environment.

The PLE values are 0.4, 0.8, and 1.5 at measurement frequencies of 19, 28, and 38 GHz, respectively. The average RMS delay spread values are 19.2, 19.3, and 20.3 ns at 19, 28, and 38 GHz, respectively. The presented results showed that the path loss and RMS delay spread are not linearly dependent. The strong received signal can be detected at a low delay spread. Finally, our results from this study, together with other propagation studies in the literature, contributes to the development of a more precise and unified channel model framework for the studied mmWave bands of 19, 28, and 38 GHz.

Author Contributions: Conceptualization, A.M.A.-S., T.A.R., M.H.A. and T.A.-H.; methodology, A.M.A.-S., T.A.R., M.H.A., T.A.-H., Y.F. and A.A.-M.; software, A.M.A.-S., T.A.R., M.H.A. and T.A.-H.; validation, A.M.A.-S., T.A.R., M.H.A., T.A.-H., Y.F. and Y.A.A.-G.; formal analysis, A.M.A.-S., T.A.R. and T.A.-H.; investigation, A.M.A.-S., T.A.R. and T.A.-H.; resources A.M.A.-S., T.A.R. and T.A.-H.; data curation, A.M.A.-S., T.A.R., T.A.-H.; writing—original draft preparation, A.M.A.-S.; writing—review and editing, A.M.A.-S., T.A.R., M.H.A., T.A.-H., Y.F., Y.A.A.-G. and A.A.-M.; visualization, A.M.A.-S., T.A.R. and T.A.-H.; supervision, T.A.R.; project administration, A.M.A.-S., T.A.R. and T.A.-H.; funding acquisition, T.A.R. and T.A.-H. All authors have read and agreed to the published version of the manuscript.

Funding: This work was supported in part by H2020-MSCA-RISE-2015 under grant 690750. This research was also funded by the Research Management Centre (RMC), Universiti Teknologi Malaysia (UTM), under the Wireless Communication Centre HICOE Grants. It was also supported by HICOE, Universiti Teknologi Malaysia (UTM) under Grant Q.J091300.23C9.00D96.

Conflicts of Interest: No conflict of interest is declared by the writers.

References

1. Pi, Z.; Khan, F. An introduction to millimeter-wave mobile broadband systems. *IEEE Commun. Mag.* **2011**, *49*, 101–107. [CrossRef]
2. Rappaport, T.S.; MacCartney, G.R.; Samimi, M.K.; Sun, S. Wideband millimeter-wave propagation measurements and channel models for future wireless communication system design. *IEEE Trans. Commun.* **2015**, *63*, 3029–3056. [CrossRef]
3. Smulders, P.F.M.; Wagemans, A.G. Wideband indoor radio propagation measurements at 58 GHz. *Electron. Lett.* **1992**, *28*, 1270. [CrossRef]
4. Geng, S.; Kivinen, J.; Zhao, X.; Vainikainen, P. Millimeter-wave propagation channel characterization for short-range wireless communications. *IEEE Trans. Veh. Technol.* **2009**, *58*, 3–13. [CrossRef]
5. Ben-Dor, E.; Rappaport, T.S.; Qiao, Y.; Lauffenburger, S.J. Millimeter-wave 60 GHz outdoor and vehicle AOA propagation measurements using a broadband channel sounder. In Proceedings of the 2011 IEEE Global Telecommunications Conference—GLOBECOM 2011, Kathmandu, Nepal, 5–9 December 2011; pp. 1–6.
6. Shafi, M.; Molisch, A.F.; Smith, P.J.; Haustein, T.; Zhu, P.; De Silva, P.; Tufvesson, F.; Benjebbour, A.; Wunder, G. 5G: A tutorial overview of standards, trials. *IEEE J. Sel. Areas Commun.* **2017**, *35*, 1201–1221. [CrossRef]
7. Al-Gumaei, Y.A.; Aslam, N.; Al-Samman, A.M.; Al-Hadhrami, T.; Noordin, K.; Fazea, Y. Non-cooperative power control game in D2D underlying networks with variant system conditions. *Electronics* **2019**, *8*, 1113. [CrossRef]
8. ITU-R. World Radiocommunication Conference 2015—Provisional Final Acts. Available online: https://www.itu.int/dms_pub/itu-r/opb/act/R-ACT-WRC.11-2015-PDF-E.pdf (accessed on 29 November 2015).
9. Durgin, G.D.; Kukshya, V.; Rappaport, T.S. Wideband measurements of angle and delay dispersion for outdoor and indoor peer-to-peer radio channels at 1920 MHz. *IEEE Trans. Antennas Propag.* **2003**, *51*, 936–944. [CrossRef]
10. Thomas, T.A.; Rybakowski, M.; Sun, S.; Rappaport, T.S.; Nguyen, H.; Kovács, I.Z. A prediction study of path loss models from 2–73.5 GHz in an urban-macro environment. In Proceedings of the 2016 IEEE 83rd Vehicular Technology Conference (Spring VTC-2016), Nanjing, China, 15–18 May 2016.
11. MacCartney, G.R.; Rappaport, T.S. Rural macrocell path loss models for millimeter wave wireless communications. *IEEE J. Sel. Areas Commun.* **2017**, *35*, 1663–1677. [CrossRef]
12. Sánchez, M.G.; Táboas, M.P.; Cid, E.L. Millimeter wave radio channel characterization for 5G vehicle-to-vehicle communications. *Measurement* **2017**, *95*, 223–229. [CrossRef]
13. Sun, S.; Rappaport, T.S.; Thomas, T.A.; Ghosh, A.; Nguyen, H.C.; Kovács, I.Z.; Rodriguez, I.; Koymen, O.; Partyka, A. Investigation of prediction accuracy, sensitivity, and parameter stability of large-scale propagation path loss models for 5G wireless communications. *IEEE Trans. Veh. Technol.* **2016**, *65*, 2843–2860. [CrossRef]

14. Faruk, N.; Bello, O.W.; Sowande, O.A.; Onidare, S.O.; Muhammad, M.Y.; Ayeni, A.A. Large scale spectrum survey in rural and urban environments within the 50 MHz—6 GHz bands. *Measurement* **2016**, *91*, 228–238. [CrossRef]
15. Alvarez, A.; Valera, G.; Lobeira, M.; Torres, R.P.; Garcia, J.L. Ultra wideband channel model for indoor environments. *J. Commun. Netw.* **2003**, *5*, 309–318. [CrossRef]
16. Maccartney, G.R.; Rappaport, T.S.; Sun, S.; Deng, S. Indoor office wideband millimeter-wave propagation measurements and channel models at 28 and 73 GHz for ultra-dense 5G wireless networks. *IEEE Access* **2015**, *3*, 2388–2424. [CrossRef]
17. Wang, Q.; Li, S.; Zhao, X.; Wang, M.; Sun, S. Wideband millimeter-wave channel characterization based on LOS measurements in an open office at 26GHz. In Proceedings of the 2016 IEEE 83rd Vehicular Technology Conference (VTC Spring), Nanjing, China, 15–18 May 2016; pp. 1–5.
18. Hur, S.; Cho, Y.-J.; Lee, J.; Kang, No.; Park, J.; Benn, H. Synchronous channel sounder using horn antenna and indoor measurements on 28 GHz. In Proceedings of the 2014 IEEE International Black Sea Conference on Communications and Networking (BlackSeaCom), Odessa, Ukraine, 27–30 May 2014; pp. 83–87.
19. Al-Samman, A.M.; Rahman, T.A.; Azmi, M.H.; Hindia, M.N.; Khan, I.; Hanafi, E. Statistical modelling and characterization of experimental mm-wave indoor channels for future 5G wireless communication networks. *PLoS ONE* **2016**, *11*, e0163034. [CrossRef] [PubMed]
20. Azar, Y.; Wong, G.N.; Wang, K.; Mayzus, R.; Schulz, J.K.; Zhao, H.; Gutierrez, F.; Hwang, D.; Rappaport, T.S. 28 GHz propagation measurements for outdoor cellular communications using steerable beam antennas in New York city. In Proceedings of the 2013 IEEE International Conference on Communications (ICC), Budapest, Hungary, 9–13 June 2013; pp. 5143–5147.
21. MacCartney, G.R.; Zhang, J.; Nie, S.; Rappaport, T.S. Path loss models for 5G millimeter wave propagation channels in urban microcells. In Proceedings of the 2013 IEEE Global Communications Conference (GLOBECOM), Atlanta, GA, USA, 9–13 December 2013; pp. 3948–3953.
22. Sun, S.; MacCartney, G.R.; Rappaport, T.S. Millimeter-wave distance-dependent large-scale propagation measurements and path loss models for outdoor and indoor 5G systems. In Proceedings of the 2016 10th European Conference Antennas Propagation (EuCAP 2016), Davos, Switzerland, 10–15 April 2016.
23. Kim, M.; Konishi, Y.; Chang, Y.; Takada, J.I. Large scale parameters and double-directional characterization of indoor wideband radio multipath channels at 11 GHz. *IEEE Trans. Antennas Propag.* **2014**, *62*, 430–441. [CrossRef]
24. Kim, M.; Umeki, K.; Wangchuk, K.; Takada, J.; Sasaki, S. Polarimetric Mm-wave channel measurement and characterization in a small office. In Proceedings of the 2015 IEEE 26th Annual International Symposium on Personal, Indoor, and Mobile Radio Communications (PIMRC), Hong Kong, China, 30 August–2 September 2015; pp. 764–768.
25. Brochure, S. Keysight Technologies 5G Channel Sounding, Reference Solution. Available online: http://about.keysight.com/en/newsroom/pr/2015/30jul-em15109.shtml (accessed on 15 September 2015).
26. Oudin, H.; Wen, Z. mmWave MIMO channel sounding for 5G: Technical challenges and prototype system. In Proceedings of the 1st International Conference on 5G for Ubiquitous Connectivity, Levi, Finland, 26–27 November 2014; pp. 192–197.
27. Rajagopal, S.; Abu-Surra, S.; Malmirchegini, M. Channel feasibility for outdoor non-line-of-sight mmWave mobile communication. In Proceedings of the 2012 IEEE Vehicular Technology Conference (VTC Fall), Quebec City, QC, Canada, 3–6 September 2012; pp. 1–6.
28. Yin, X.; He, Y.; Song, Z.; Kim, M.-D.; Chung, H.K. A sliding-correlator-based SAGE algorithm for Mm-wave wideband channel parameter estimation. In Proceedings of the 8th European Conference on Antennas and Propagation (EuCAP 2014), Hague, The Netherlands, 6–11 April 2014; pp. 625–629.
29. Fessler, J.A.; Hero, A.O. Space-alternating generalized expectation-maximization algorithm. *IEEE Trans. Signal Process.* **1994**, *42*, 2664–2677.
30. Piersanti, S.; Annoni, L.A.; Cassioli, D. Millimeter waves channel measurements and path loss models. In Proceedings of the 2012 IEEE International Conference on Communications (ICC), Ottawa, ON, Canada, 10–15 June 2012; pp. 4552–4556.
31. Rappaport, T.S. *Wireless Communications Principles and Practice*, 2nd ed.; Prentice Hall: Upper Saddle River, NJ, USA, 2002.

32. Rappaport, T.S.; Ben-Dor, E.; Murdock, J.N.; Qiao, Y. 38 GHz and 60 GHz angle-dependent propagation for cellular & peer-to-peer wireless communications. In Proceedings of the IEEE International Conference on Communications, Ottawa, ON, Canada, 10–15 June 2012; pp. 4568–4573.
33. Deng, S.; Samimi, M.K.; Rappaport, T.S. 28 GHz and 73 GHz millimeter-wave indoor propagation measurements and path loss models. In Proceedings of the 2015 IEEE International Conference on Communication Workshop (ICCW), London, UK, 8–12 June 2015; pp. 1244–1250.